

LEVEL

(P)
PS

1-
AD A101378

Properties of the Channel Electron Multiplier Arrays (CEMAs) for the SOLEX Solar X-Ray Spectrometer/Spectroheliograph

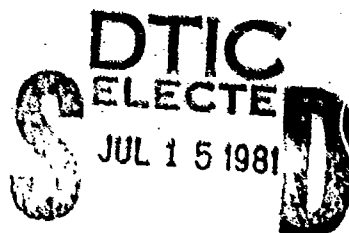
E. ENG, JR. and P. B. LANDECKER
Space Sciences Laboratory
Laboratory Operations
The Aerospace Corporation
El Segundo, Calif. 90245

15 June 1981

APPROVED FOR PUBLIC RELEASE;
DISTRIBUTION UNLIMITED

DTIC FILE COPY

Prepared for
SPACE DIVISION
AIR FORCE SYSTEMS COMMAND
Los Angeles Air Force Station
P.O. Box 92960, Worldwide Postal Center
Los Angeles, Calif. 90009



A

81 7 13 083

This report was submitted by The Aerospace Corporation, El Segundo, CA 90245, under Contract No. F04701-80-C-0081 with the Space Division, Deputy for Technology, P.O. Box 92960, Worldway Postal Center, Los Angeles, CA 90009. It was reviewed and approved for The Aerospace Corporation by G. A. Paulikas, Director, Space Sciences Laboratory. Lt R. S. Weidenheimer, SD/YLVS, was the project officer for Mission-Oriented Investigation and Experimentation (MOIE) Programs.

This report has been reviewed by the Public Affairs Office (PAS) and is releasable to the National Technical Information Service (NTIS). At NTIS, it will be available to the general public, including foreign nations.

This technical report has been reviewed and is approved for publication. Publication of this report does not constitute Air Force approval of the report's findings or conclusions. It is published only for the exchange and stimulation of ideas.

Randall S. Weidenheimer
Randall S. Weidenheimer, 2nd Lt., USAF
Project Officer

Florian P. Meinhardt
Florian P. Meinhardt, Lt. Col.
USAF Director of Advanced Space
Development

FOR THE COMMANDER

William Goldberg
William Goldberg, Col., USAF
Deputy for Technology

UNCLASSIFIED

SECURITY CLASSIFICATION OF THIS PAGE (When Data Entered)

REPORT DOCUMENTATION PAGE		READ INSTRUCTIONS BEFORE COMPLETING FORM
1. REPORT NUMBER SD/TR-81-55	2. GOVT ACCESSION NO. AD-101378	3. RECIPIENT'S CATALOG NUMBER
4. TITLE (and Subtitle) PROPERTIES OF THE CHANNEL ELECTRON MULTIPLIER ARRAYS (CEMAS) FOR THE SOLEX SOLAR X-RAY SPECTROMETER/SPECTROHELIOPHOTOGRAPH		5. TYPE OF REPORT & PERIOD COVERED
6. AUTHOR(s) W. Eng, Jr. and P. B. Landecker		7. PERFORMING ORG. REPORT NUMBER TR-0081(6960-01)-3
8. PERFORMING ORGANIZATION NAME AND ADDRESS The Aerospace Corporation El Segundo, Calif. 90245		9. CONTRACT OR GRANT NUMBER(s) F04701-80-C-0081
10. PROGRAM ELEMENT, PROJECT, TASK AREA & WORK UNIT NUMBERS 1148		11. CONTROLLING OFFICE NAME AND ADDRESS Space Division Air Force Systems Command Los Angeles, Calif. 90009
12. REPORT DATE 15 June 1981		13. NUMBER OF PAGES 40
14. MONITORING AGENCY NAME & ADDRESS (if different from Controlling Office)		15. SECURITY CLASS. (of this report) Unclassified
16. DISTRIBUTION STATEMENT (of this Report) Approved for public release; distribution unlimited		17. DECLASSIFICATION/DOWNGRADING SCHEDULE
18. DISTRIBUTION STATEMENT (of the abstract entered in Block 30, if different from Report)		
19. SUPPLEMENTARY NOTES		
20. KEY WORDS (Continue on reverse side if necessary and identify by block number) Channel Electron Multiplier Arrays X-ray Detectors		
21. ABSTRACT (Continue on reverse side if necessary and identify by block number) A Channel Electron Multiplier Array (CEMA) detector was launched on 24 February 1979 as part of the SOLEX Solar X-Ray Spectrometer/Spectroheliograph experiment aboard the U.S. Air Force Space Test Program P78-1 satellite. Since launch, this detector has successfully recorded X-rays in the 3-25 Å wavelength range. This report describes the comprehensive laboratory testing program of the flight and flight spare CEMA detectors. Quantum efficiencies, energy resolution and gain are given as a function of different incident		

UNCLASSIFIED

SECURITY CLASSIFICATION OF THIS PAGE(When Data Entered)

19. KEY WORDS (Continued)

20. ABSTRACT (Continued)

~~✓~~ photon wavelengths, voltage configurations, incident angles and lifetime exposures. Our results are compared to other published values.

UNCLASSIFIED

SECURITY CLASSIFICATION OF THIS PAGE(When Data Entered)

PREFACE

The authors thank Drs. J. P. Henry, D. L. McKenzie, H. R. Rugge, J. G. Timothy, J. H. Underwood and J. Wiza for their many helpful discussions. C. K. Howey and R. L. Williams provided the supporting mechanical and electrical designs, respectively.

✓
A

CONTENTS

PREFACE.....	1
I. INTRODUCTION.....	7
II. EXPERIMENTAL SETUP.....	9
III. TESTING.....	9
IV. SUMMARY AND CONCLUSIONS.....	33
REFERENCES.....	37

FIGURES

1. CEMA Experimental Setup.....	8
2. CEMA/X-ray Source Setup.....	10
3. CEMA #101 Quantum Efficiency versus Angular Position (between CEMA normal and collimated X-ray beam).....	11
4. Gain versus Total Pulse Height Analyzer Counts from CEMA #101 in the Flight Configuration.....	13
5. Quantum Efficiency versus Total Pulse Height Analyzer Counts from CEMA #101 in the Flight Configuration.....	14
6. Full Width at Half Maximum versus Total Pulse Height Analyzer Counts from CEMA #101 in the Flight Configuration.....	15
7. Dark Counting Rate (background rate) versus Total Pulse Height Analyzer Counts from CEMA #101 in the Flight Configuration.....	16
8. Full Width at Half Maximum versus $V_{front} - V_{shield}$ for CEMA #101. ($V_{middle\ top} - V_{middle\ bottom} = 20$ volts and $V_{collector} - V_{shield} = 2700$ volts).....	17
9. Quantum Efficiency versus $V_{front} - V_{shield}$ for CEMA #101 ($V_{middle\ top} - V_{middle\ bottom} = 20$ volts and $V_{collector} -$ $V_{shield} = 2700$ volts).....	18
10. Full Width at Half Maximum versus $V_{middle\ top} - V_{middle\ bottom}$ for CEMA #101.....	19
11. Quantum Efficiency versus $V_{middle\ top} - V_{middle\ bottom}$ for CEMA #101 ($V_{front} - V_{shield} = 0$ volts and $V_{collector} -$ $V_{shield} = 2700$ volts).....	20
12. Gain versus $V_{collector} - V_{shield}$ for CEMA #101.....	22
13. Full Width at Half Maximum versus $V_{collector} - V_{shield}$ for CEMA #101.....	23

FIGURES (Continued)

14. Quantum Efficiency versus Wavelength for CEMA #101 with Shield #1 Present..... 24
15. Full Width of Half Maximum versus Wavelength for CEMA #101 ($V_{front} - V_{shield} = 0$ volts and $V_{middle\ top} - V_{middle\ bottom} = 0$ volts)..... 25
16. Quantum Efficiency versus Angular Position (between CEMA normal and X-ray beam) for CEMA #101..... 27
17. Comparison of CEMA Quantum Efficiency versus Wavelength to that of Other Investigators..... 28
18. Gain versus Dose for Two Different Types of Plates Tested by Henry et al..... 29
19. Quantum Efficiency versus Angular Position (between CEMA normal and X-ray beam) for CEMA #102..... 31
20. Quantum Efficiency versus Wavelength for CEMA #102 (corrected for the effects of shield #9) in the Flight Configuration with Appropriate Error Bars and Absorption Edges Shown..... 32
21. Quantum Efficiency versus Wavelength for CEMA #101 (taking absorption edges into account) in the Flight Configuration with Shield #10 and #12 Present..... 34
22. Comparison of CEMA #101 Quantum Efficiency versus Wavelength (taking absorption edges into account) with that of Other Investigators..... 35

I. INTRODUCTION

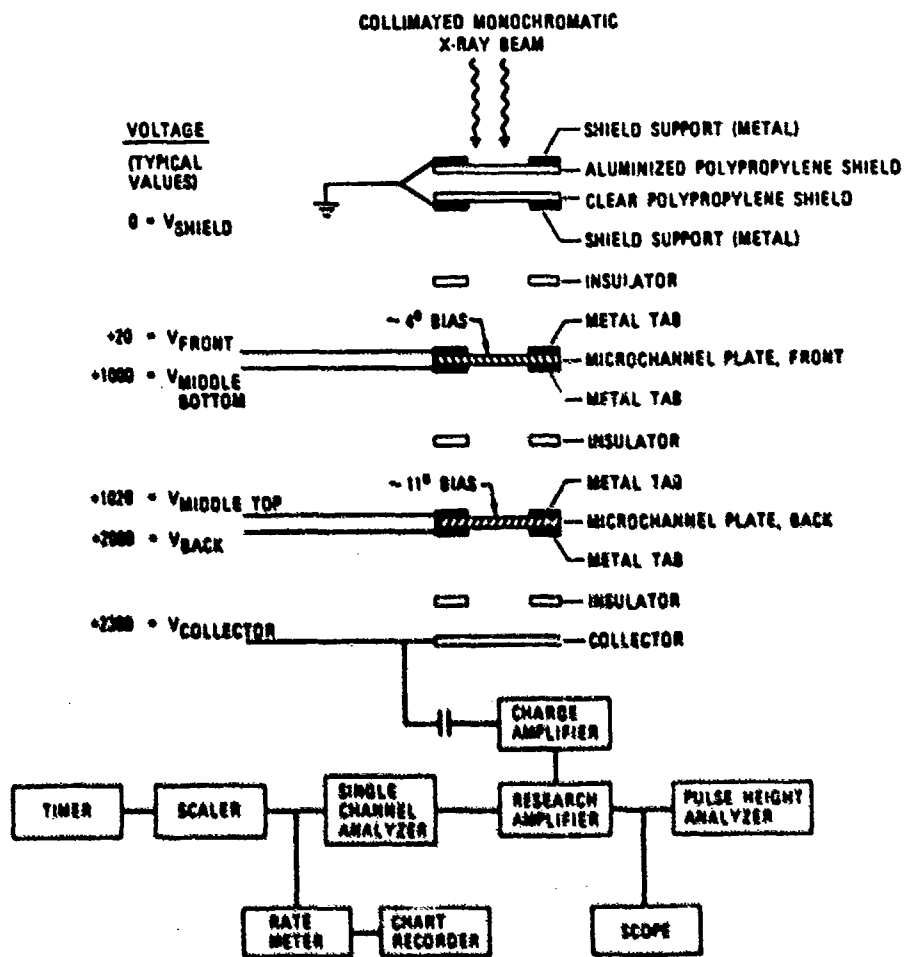
The SOLEX Solar X-Ray Spectrometer/Spectroheliograph payload was launched in the pointed section of the U.S. Air Force Space Test Program P78-1 satellite on 24 February 1979 and is currently obtaining solar raster maps in individual x-ray spectral lines and recording spectra in the 3-25 Å wavelength interval with excellent spectral, spatial and temporal resolution (Landecker et al., 1979a, 1979b, 1980; McKenzie et al., 1980a, 1980b, 1981; Landecker and McKenzie, 1980; Doschek et al., 1981). A sealed proportional counter detector is sensitive only up to about 14 Å. In order to detect the many x-ray lines above 14 Å, given the constraint that flow counter systems were not permitted, we selected as one SOLEX detector a CEMA (for Channel Electron Multiplier Array) device.

The Galileo Chevron CEMA is a high gain, low noise x-ray sensitive detector that consists of two plates of straight, narrow tubes that are separated by an insulator (Wiza, 1979). The tubes in the plates are biased with respect to each other; this dramatically reduces the problem of ion feedback which, if present, would appear as spurious background.

The orientation of channels in the plates is shown in Figure 1. The length of the CEMA tubes was chosen to obtain a large channel length to channel diameter (L/D) ratio. An L/D ratio of 86 was selected to achieve a better pulse height distribution (i.e. detector resolution) at the desired high electron gain, and to minimize gain variations between individual microchannels. The bias angle between the CEMA channels and the normal to the front plate was determined by Galileo to be $30^\circ 45' \pm 10'$.

On the low voltage side of the CEMA there is located an assembly consisting of aluminized and clear polypropylene filters to block solar EUV and UV radiation and electrons, to serve as a Faraday shield, and to keep the CEMA clean during prelaunch tests and handling (Landecker and Eng, 1978). A coating of magnesium fluoride on the CEMA cathode was used to increase the quantum efficiency.

This report describes the results of extensive testing of the flight and flight spare CEMA detectors.



1. CERIA Experimental Setup. V_{shield} to V_{front} was variable from 0 to 50 volts. $V_{\text{middle bottom}}$ to $V_{\text{middle top}}$ was variable from 1000 to 1050 volts. Laboratory tests were conducted in order to determine the optimum flight configuration.

II. EXPERIMENTAL SETUP

An X-ray source consisting of a Henke tube, a rotary fluorescent target wheel and a mechanical collimator was used to determine the pertinent characteristics of the Galileo CEMAs. The x-ray energies produced by the source included

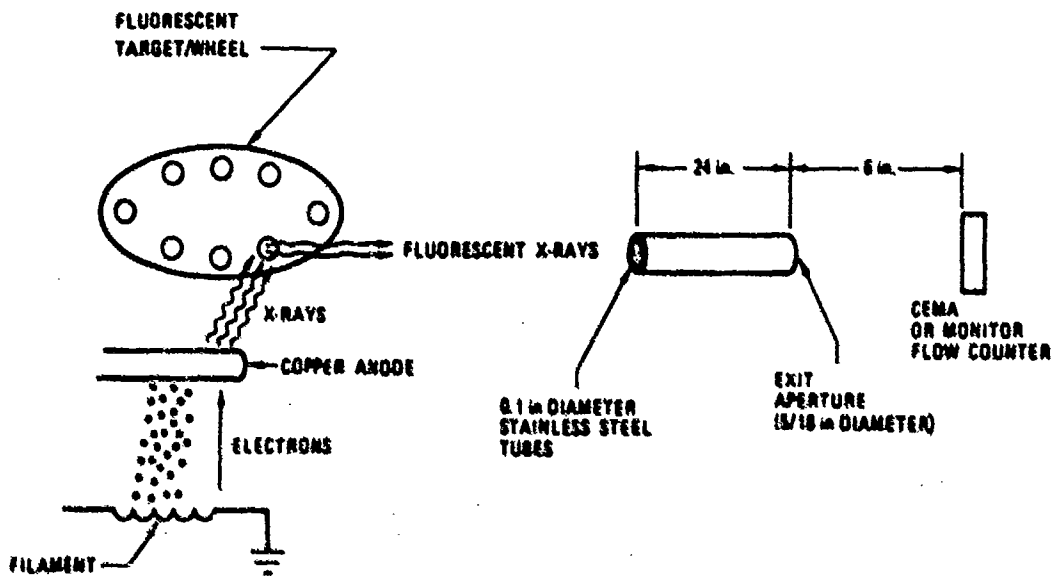
FeKa (1.937 Å)	CrKa (2.291 Å)	TiKa (2.750 Å)	SnLa (3.600 Å)
AgLa (4.154 Å)	MoLa (5.406 Å)	SrLa (6.862 Å)	SiKa (7.126 Å)
AlKa (8.338 Å)	SeLa (8.990 Å)	MgKa (9.889 Å)	GeLa (10.44 Å)
ZnLa (12.26 Å)	CuLa (13.33 Å)	NiLa (14.57 Å)	CoLa (15.97 Å)
FeLa (17.57 Å)	FeKa (18.32 Å)	MnLa (19.45 Å)	CrLa (21.67 Å)
OKa (23.71 Å)	VLa (24.26 Å)	TiLa (27.39 Å)	

The x-rays were collimated by a number of stainless steel tubes of 0.1" diameter and 24" length. The full width collimation of the source was 0.24° while the circular beam exiting the collimator was 5/16" in diameter. This collimated monochromatic x-ray beam was alternately allowed to intercept the CEMA under test and a flow proportional counter monitor of known efficiency. The x-ray source configuration is shown schematically in Figure 2.

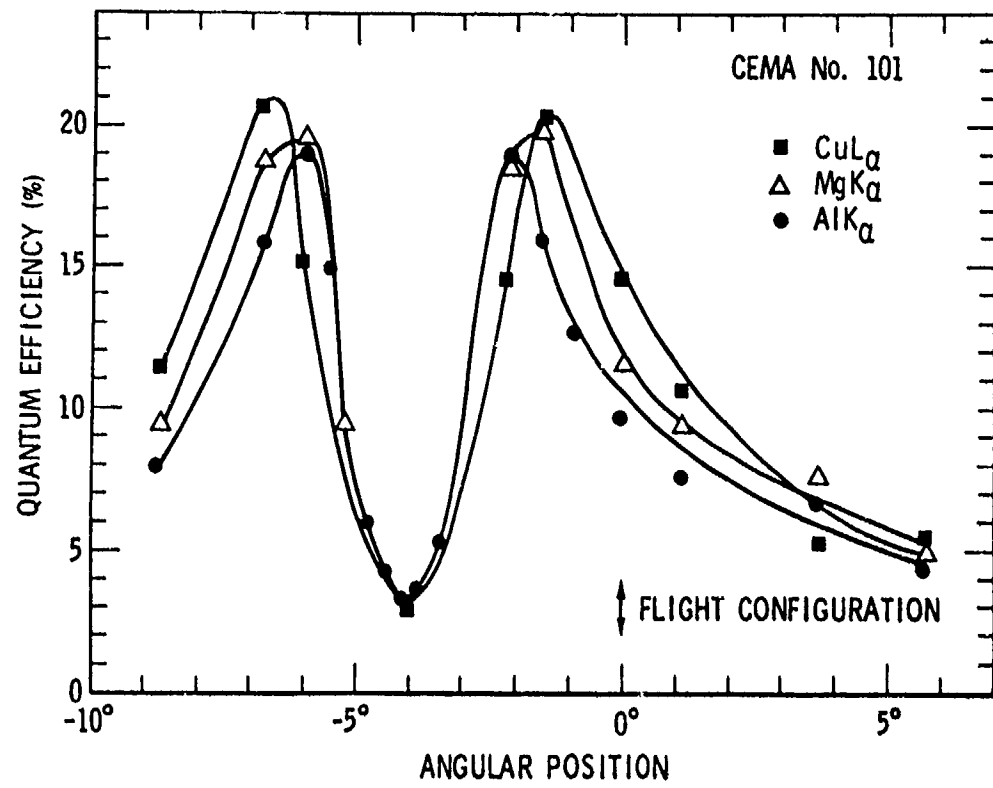
III. TESTING

Data was taken to determine the quantum efficiency (Q.E.) of CEMA #101 (currently aboard P78-1 satellite) and flight spare CEMA #102 as a function of the angle of incidence between the CEMA normal and x-ray beam from the collimator. The CMAs were mounted so that the normal to the front plate was approximately parallel to the x-ray beam while the rotary table on which the CEMA was attached could be rotated by $\pm 7^\circ$. The data for CEMA #101 are plotted in Figure 3. The Q.E. is a minimum when the x-ray beam points directly down the tubes of the front plate.

The graph of quantum efficiency versus wavelength for different angular positions shows a maximum when the angle between the CEMA channels and the x-ray beam is approximately 2.6°. A fairly good efficiency is obtained for wavelengths Al Ka, MgKa, and CuLa at the angular configuration where the CEMA channels are 4° to the x-ray beam. This point is indicated by the arrow



2. CERIA/X-ray Source Setup. Monochromatic, collimated X-ray beams produced by the source were used to calibrate the CEMAs.



3. CEMA #101 Quantum Efficiency versus Angular Position (between CEMA normal and collimated X-ray beam). High voltage = 2700 volts (between shield and collector). $V_{\text{front}} - V_{\text{shield}} = 30$ volts. $V_{\text{middle top}} - V_{\text{middle bottom}} = 20$ volts. Q.E. includes absorption by shield #1 (1.2 μm polypropylene and 250 nm aluminum).

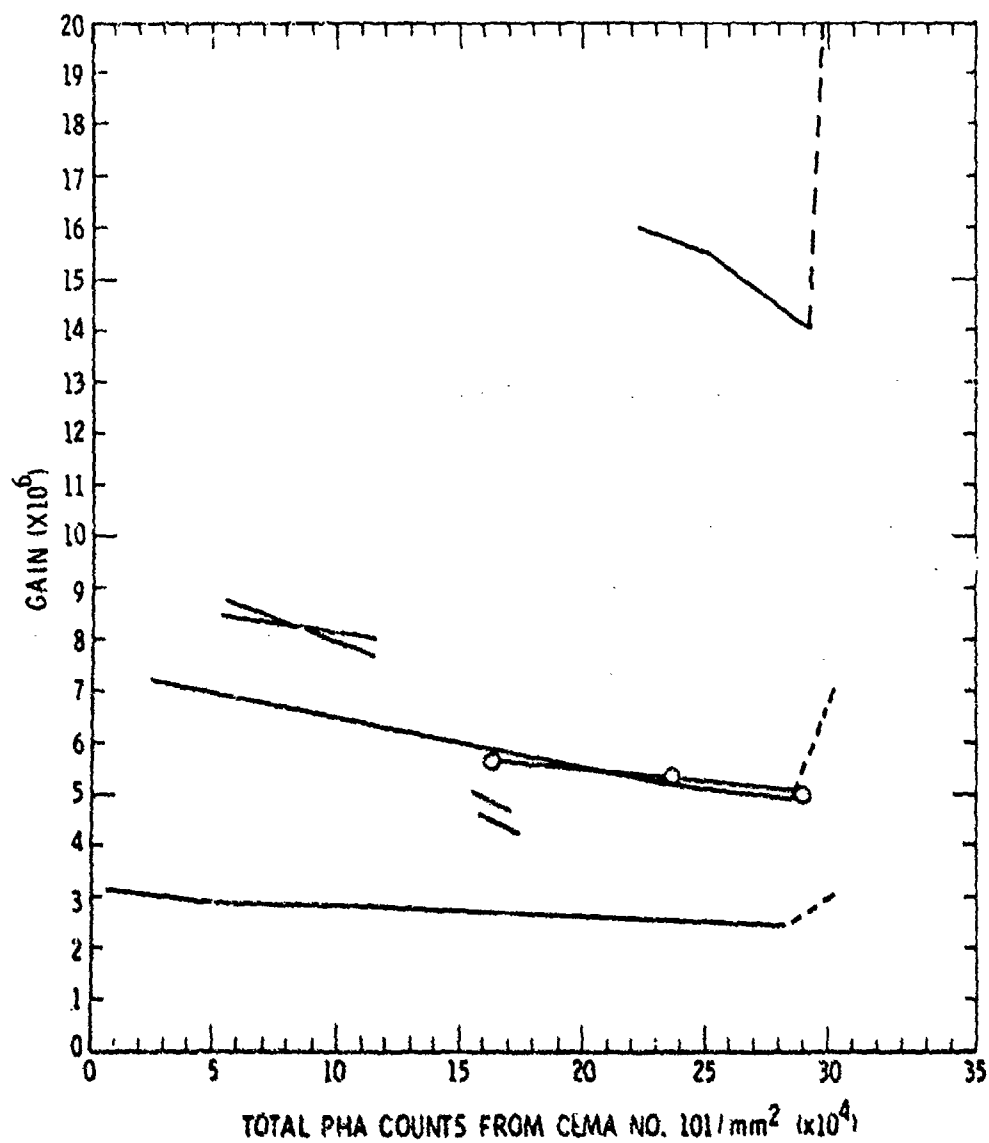
at 0° in Figure 3 and is called the flight configuration. (It should be noted that the flight configuration, with reference to Figure 1, means that $V_{\text{front}} = V_{\text{shield}} = 0$ Volts, and $V_{\text{middle top}} - V_{\text{middle bottom}} = 0$ Volts.) The optimum angle of about 4° between the incident photon (X-ray) beam and the front channels resulted in a reasonable compromise between quantum efficiency and resolution.

Tests were performed to measure the detector degradation as a function of exposure. An analysis of CEMA #101 shows that pertinent parameters can be plotted versus the total number of pulses counted by the pulse height analyzer (FHA). The source beam is collimated so that all X-rays hit one spot on this CEMA and form a circular impact area 0.46 inches in diameter.

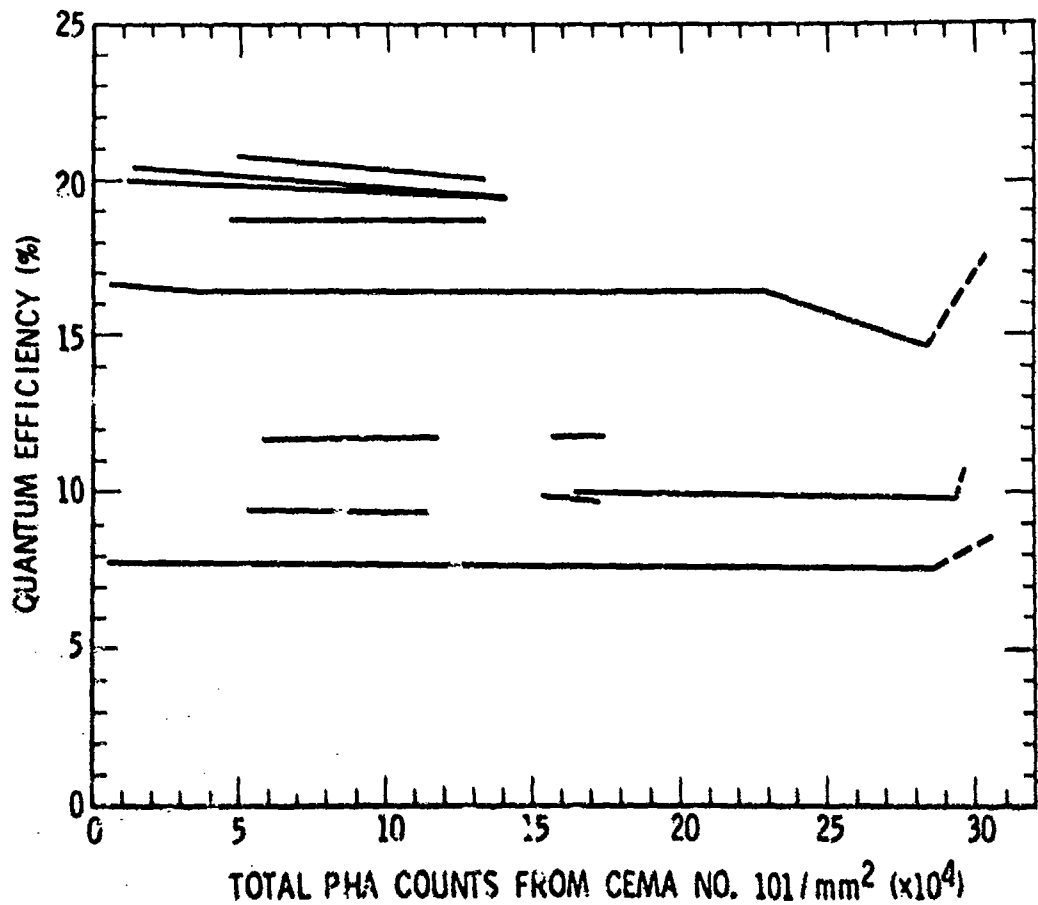
Figure 4 which gives the CEMA gain versus total PHA counts shows that the gain linearly decreases with total pulses. As shown in Figure 5, the Q.E. versus total PHA counts tends to slowly decrease with total counts. The FWHM (Full Width at Half Maximum) (%) resolution of the counter versus total PHA counts (Figure 6) tends to decrease slightly with total counts. At the same time, the dark counting rate in general tends to increase with total counts (Figure 7). At the end of all these lifetime tests, a new data point was plotted on all graphs by illuminating a region on the CEMA which previously had not been exposed to radiation. The data shows that the new spot on CEMA #101 had an increase in gain and Q.E. but that there was no particular difference with regard to FWHM (%) or dark counting rate. The new points are given in Figures 4-7 (dashed lines).

Data was also taken to determine the effect of applying a voltage between the shield and front plate; the voltage was varied between 0 and 50 volts. This was done to see if the detector resolution or quantum efficiency would improve. The resolution does improve slightly as the applied voltage increases to near 50 volts. However, the quantum efficiency remains constant. The effect is plotted in Figures 8 and 9.

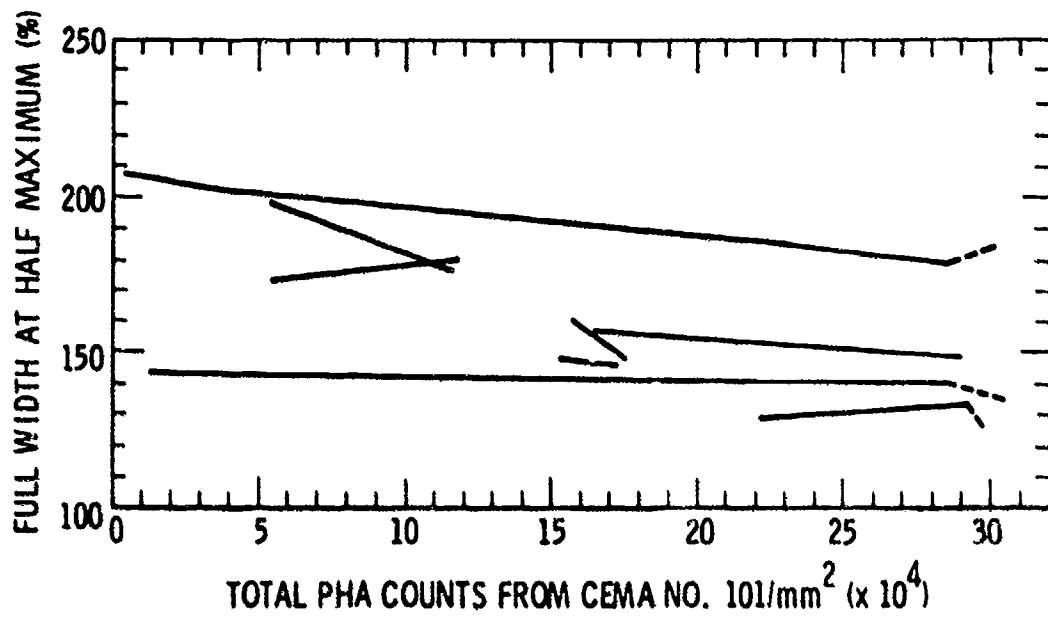
A voltage (20-50 volts) was also applied between the middle bottom tab and the middle top tab to see if the resolution or quantum efficiency could be improved. As shown in Figure 10, the resolution does improve as the applied voltage increases. However, as shown in Figure 11, the quantum efficiency again remains constant.



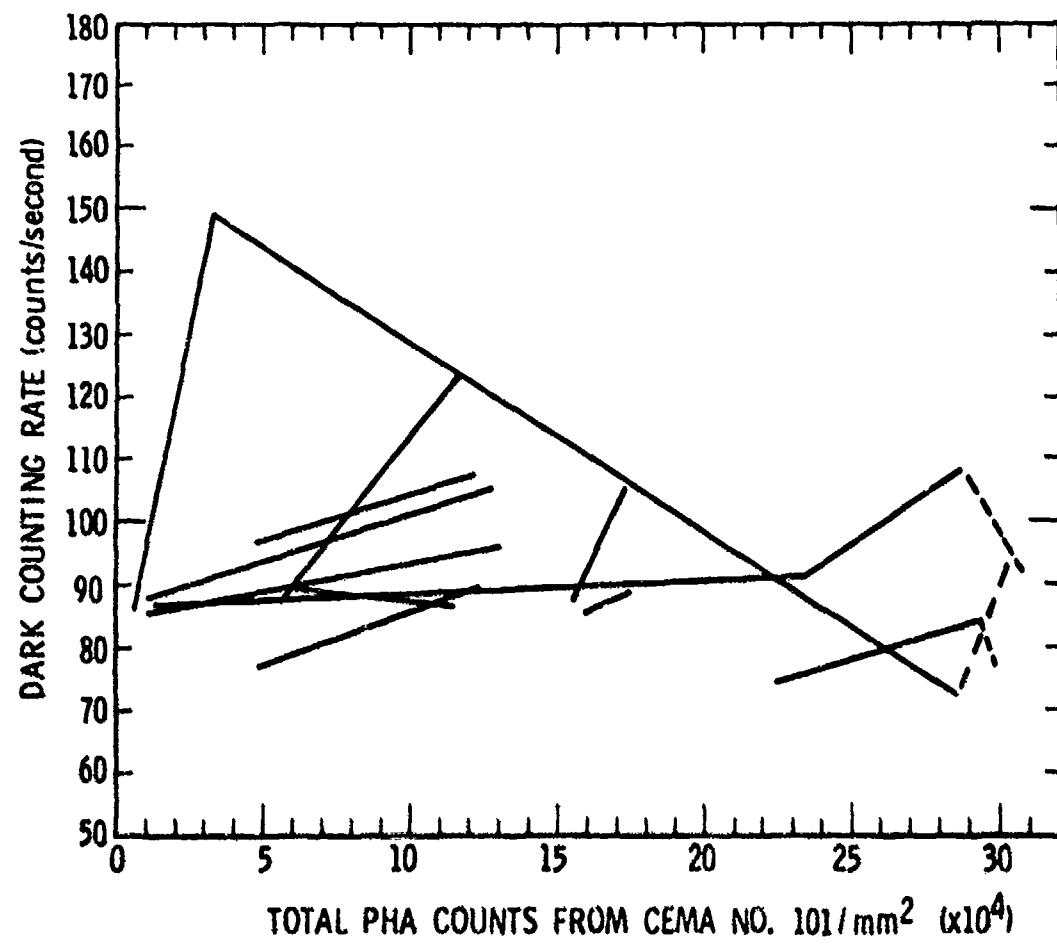
4. Gain versus total pulse height analyzer counts from CEMA #101 in the flight configuration. The dashed lines show the gain change when X-rays are incident upon a different section of the CEMA previously free from radiation. Several combinations of wavelengths, voltages and incident angles are shown.



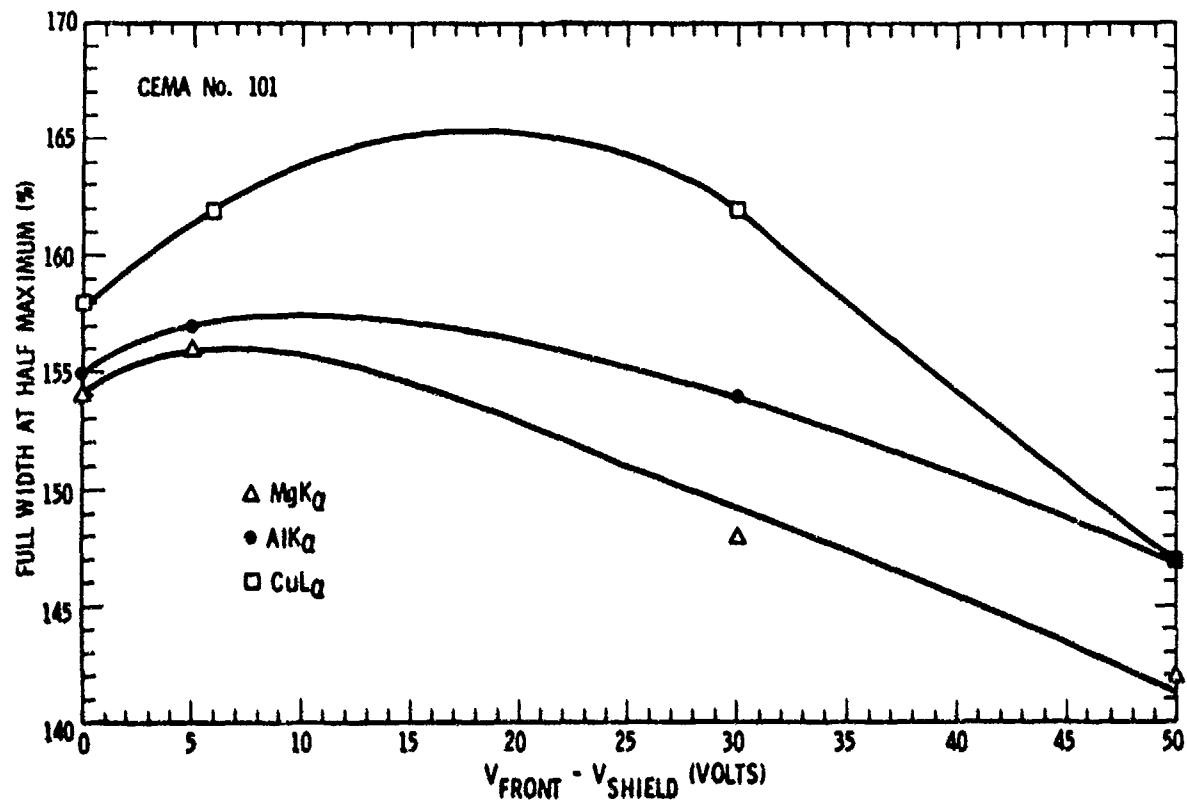
5. Quantum efficiency versus total pulse height analyzer counts from CEMA #101 in the flight configuration. The dashed lines show the Q.E. change when X-rays hit a different section of the CEMA previously free from radiation. Several combinations of wavelengths, voltages and incident angles are shown.



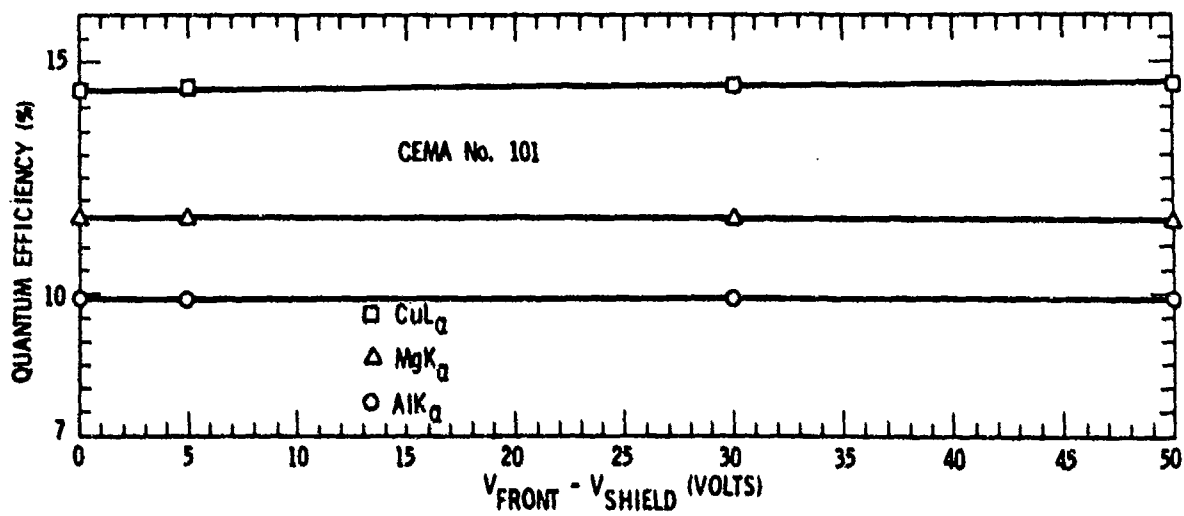
6. Full width at half maximum versus total pulse height analyzer counts from CEMA #101 in the flight configuration. The dashed lines show the resolution change when X-rays hit a different section of the CEMA previously free from radiation. Several combinations of wavelengths, voltages and incident angles are shown.



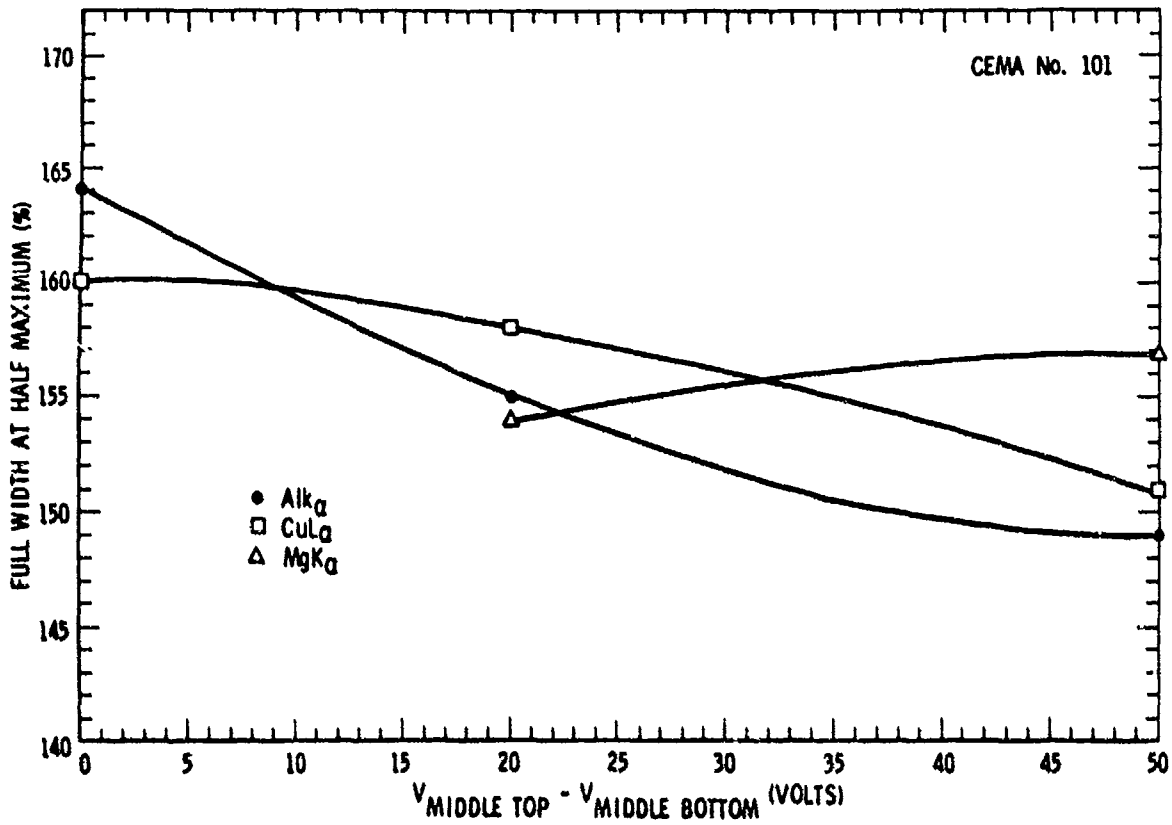
7. Dark counting rate (background rate) versus total pulse height analyzer counts from CEMA #101 in the flight configuration. The dashed lines show the resolution change when X-rays hit a different section of the CEMA previously free from radiation. Several combinations of wavelengths, voltages and incident angles are shown.



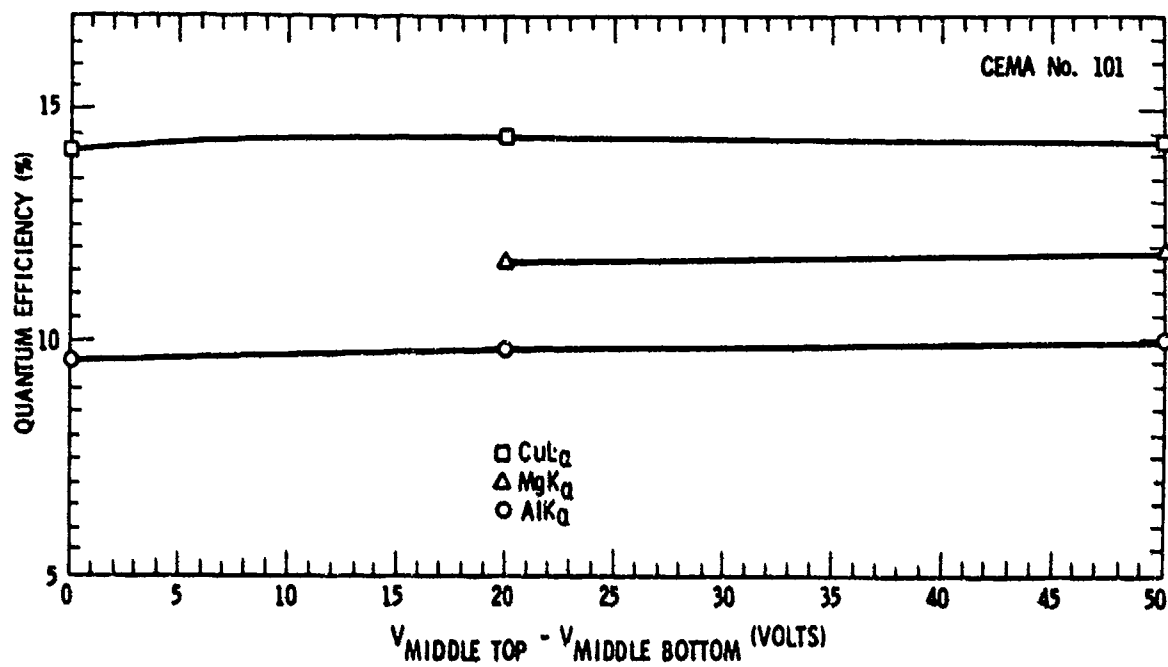
8. Full width at half maximum versus $V_{front} - V_{shield}$ for CEMA #101. ($V_{middle top} = V_{middle bottom} = 20$ volts and $V_{collector} = V_{shield} = 2700$ volts).



9. Quantum efficiency versus $V_{front} - V_{shield}$ for CEMA #101 ($V_{middle\ top} - V_{middle\ bottom} = 20$ volts and $V_{collector} - V_{shield} = 2700$ volts). Shield #1 was present on the CEMA.



10. Full width at half maximum versus $V_{middle\ top} - V_{middle\ bottom}$ for CEMA #101. ($V_{front} - V_{shield} = 0$ volts and $V_{collector} - V_{shield} = 2700$ volts).



11. Quantum efficiency versus $V_{\text{middle top}} - V_{\text{middle bottom}}$ for CEMA #101
 $(V_{\text{front}} - V_{\text{shield}} = 0$ volts and $V_{\text{collector}} - V_{\text{shield}} = 2700$ volts). Shield #1 was present on the CEMA.

The extent to which our resolution improves as the applied voltage increases differs from that reported by J. L. Wiza (1977). In applying 50 volts between the middle top tab and middle bottom tab, we improved our resolution from 160 to 150%, whereas, Wiza was able to improve his resolution from 160 to 110%. There are two possible reasons for this disparity of results. We used X-rays while Wiza used UV excitation and the CEMA devices could have been manufactured to different specifications.

In both of the tests above where voltages were varied, the gain of the CEMA became lower as the differences ($V_{front} - V_{shield}$ or $V_{middle\ top} - V_{middle\ bottom}$) increased. This effect was due to the net voltage across the plates decreasing at the same time.

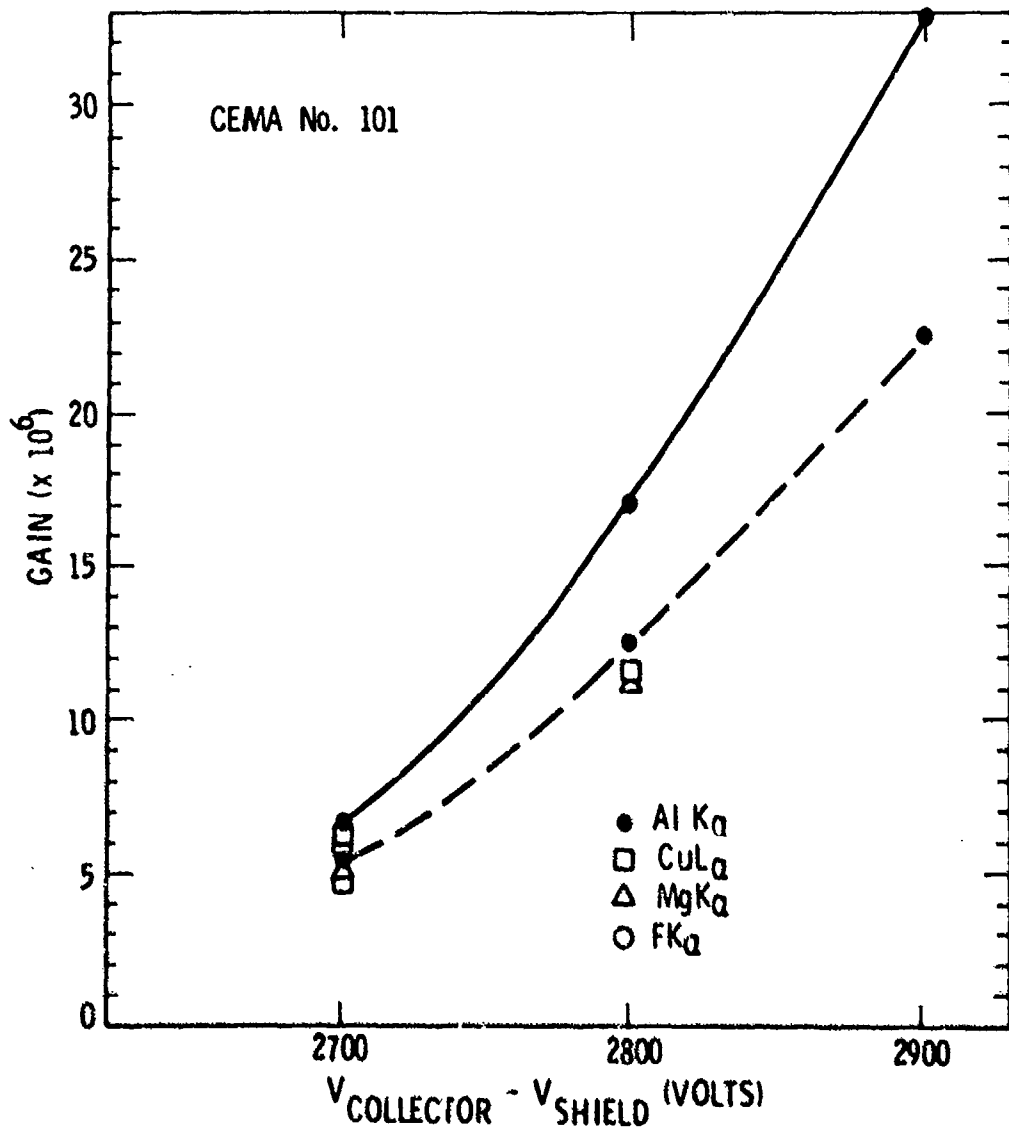
Data was also taken in Al Ka, CuKa, and FKa to determine the CEMA gain as a function of the voltage from the shield to the collector for the case where $V_{middle} - V_{front} = V_{back} - V_{middle} = I_{CEMA} \times (4.5 \text{ megohm})$ and $V_{collector} - V_{back} = I_{CEMA} \times (1.3 \text{ megohm})$. The results show a fairly linear behavior as can be seen in Figure 12.

Also, the resolution (%FWHM) versus the voltage across the shield to collector for the case where $V_{middle} - V_{front} = V_{back} - V_{middle} = I_{CEMA} \times (4.5 \text{ megohm})$ and $V_{collector} - V_{back} = I_{CEMA} \times (1.3 \text{ megohm})$ was measured. The results show the resolution is improved as the voltage across the CEMA (shield to collector) increases. However, the counter lifetime probably also decreases as the tube gain is increased (Figure 13).

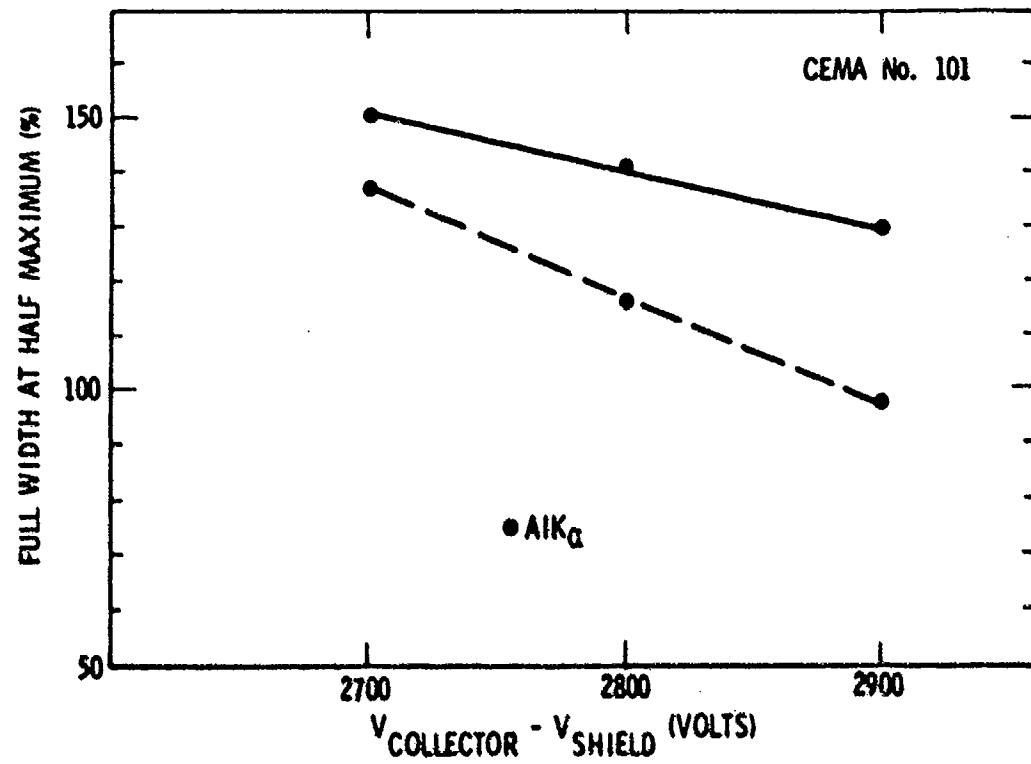
Upon reviewing the data obtained when varying the voltages across the CEMA ($V_{middle\ top} - V_{middle\ bottom}$ and $V_{front} - V_{shield}$), it was decided to adopt the "flight" configuration in order to maximize the detector simplicity and, therefore, the post-launch reliability, since the voltage refinements did not substantially improve our measured performance of CEMA #101.

Figure 14 shows the quantum efficiency versus wavelength (at Al Ka, MgKa, and CuKa) for different angles between the x-ray beam and the CEMA channels.

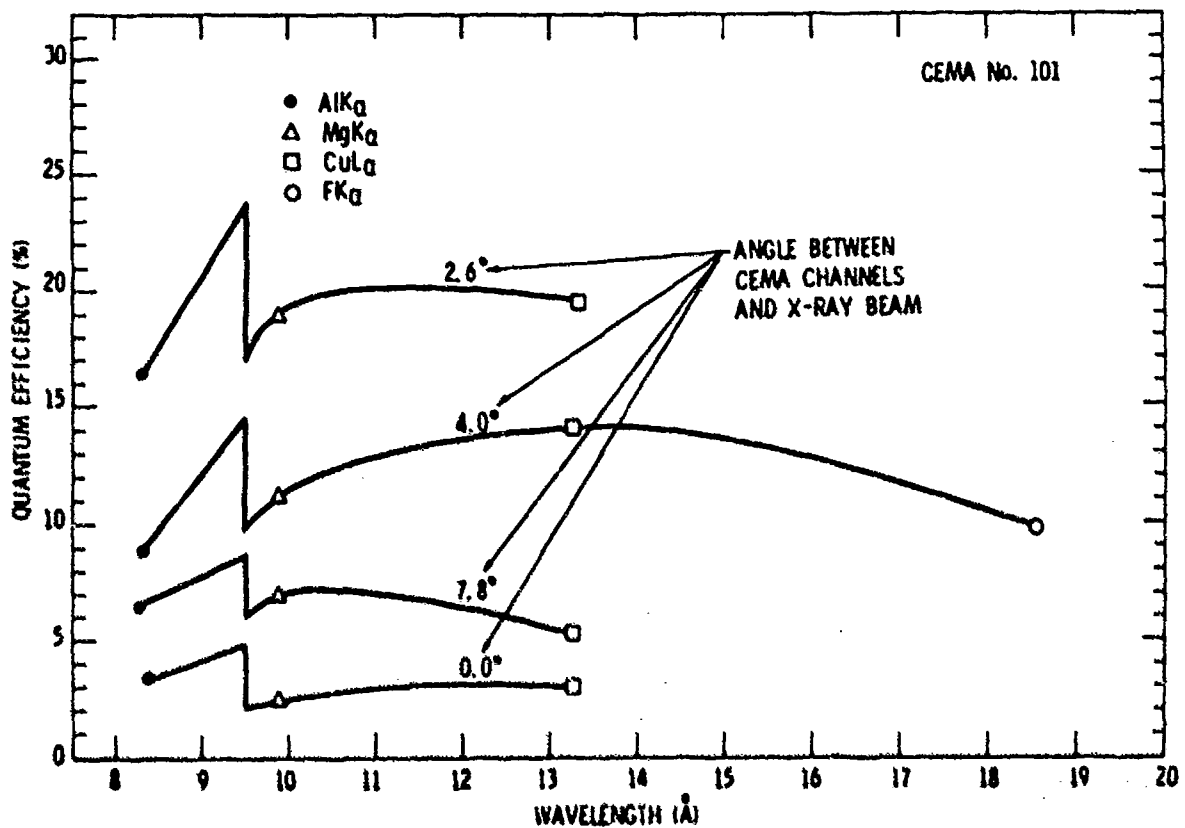
Figure 15 shows the resolution versus wavelength for different angles between CEMA channels and x-ray beam, and different voltages across the CEMA.



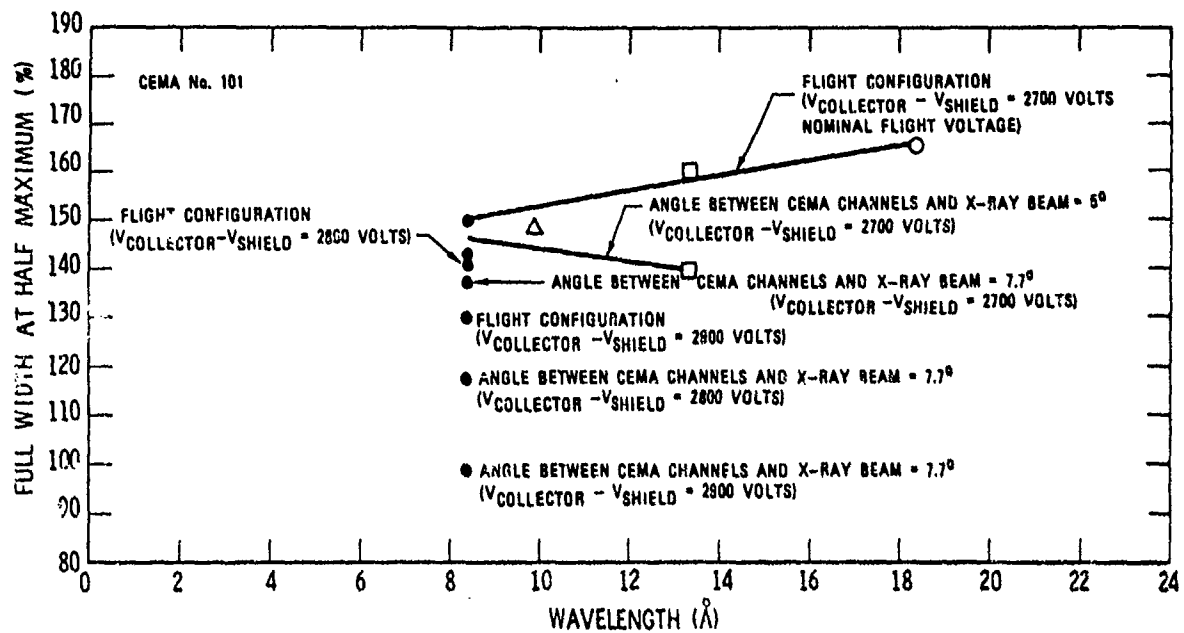
12. Gain versus $V_{collector} - V_{shield}$ for CEMA #101. The two Al Ka cases shown are the flight configuration ($V_{front} - V_{shield} = 0$ volts and $V_{middle top} - V_{middle bottom} = 0$ volts) and the situation where $V_{front} - V_{shield} = 0$ volts and $V_{middle top} - V_{middle bottom} = 20$ volts (dashed line). In both cases the X-rays are incident approximately 4° to the CEMA channels. Data points for other lines are shown for the flight configuration.



13. Full width at half maximum versus $V_{\text{collector}} - V_{\text{shield}}$ for CEMA #101. The two cases shown are the flight configuration ($V_{\text{front}} = V_{\text{shield}} = 0$ volts and $V_{\text{middle top}} = V_{\text{middle bottom}} = 0$ volts with the angle between CEMA channels and X-ray beam approximately 4°) and the situation where $V_{\text{front}} - V_{\text{shield}} = 0$ volts and $V_{\text{middle top}} - V_{\text{middle bottom}} = 0$ volts with the angle between CEMA channels and X-ray beam approximately 8.1° (dashed line).



14. Quantum efficiency versus wavelength for CEMA #101 with shield #1 present. The four curves show the Q.E. for the cases of different angles between CEMA channels and X-ray beam. The effects of absorption edges have been included.



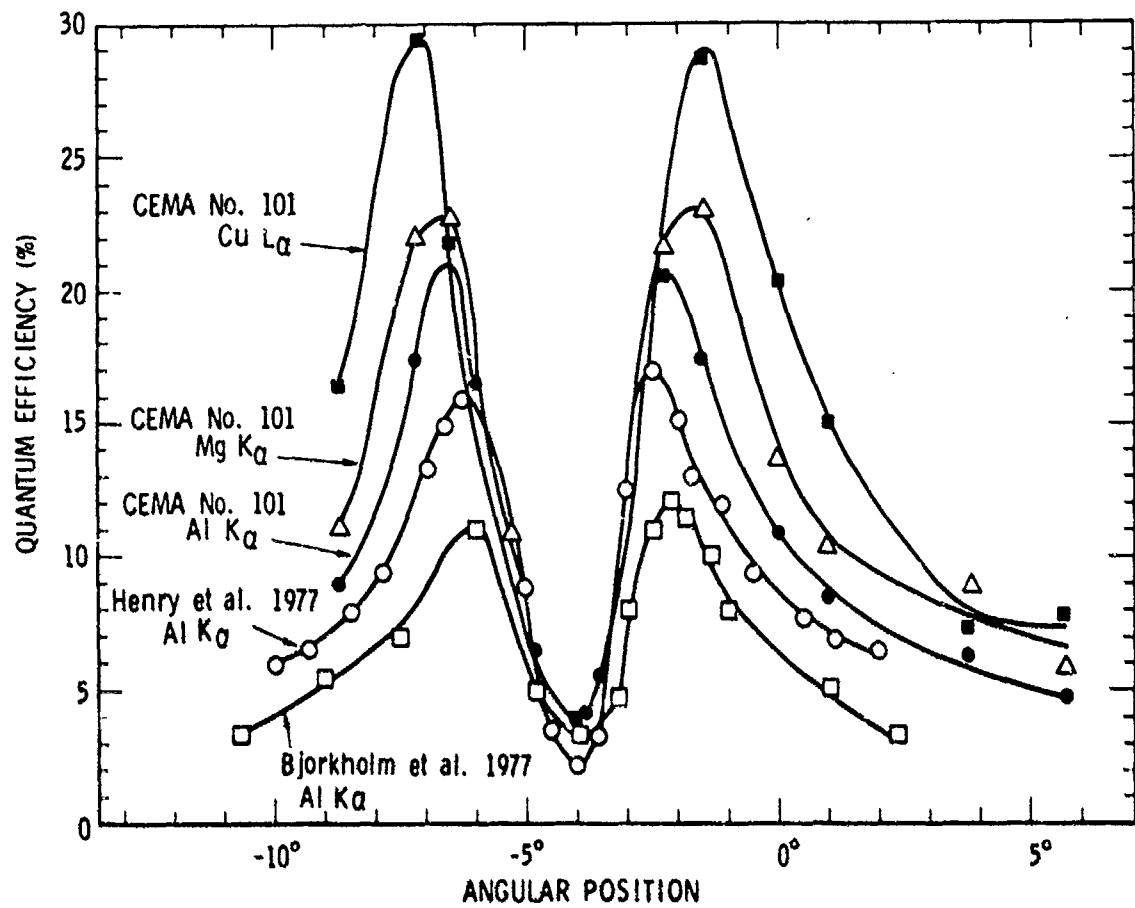
15. Full width of half maximum versus wavelength for CEMA #101 ($V_{front} - V_{shield} = 0$ volts and $V_{middle\ top} - V_{middle\ bottom} = 0$ volts).

In Figure 16 we compare our measurements of the quantum efficiency versus angular position for CEMA #101 to similar measurements by two other experimenters. It is seen that for Al K α , the Q.E. for #101 is higher overall than that for either Henry et al (1977) or Bjorkholm et al (1977). This higher Q.E. for all angular positions may be due to a different glass composition or cathode coating of our CEMA than that used by Henry et al. and Bjorkholm et al. It should be noted that Henry et al. used a coated Mullard plate while Bjorkholm et al. used an uncoated Mullard plate. The full width beam spread of the Bjorkholm test was 1°.

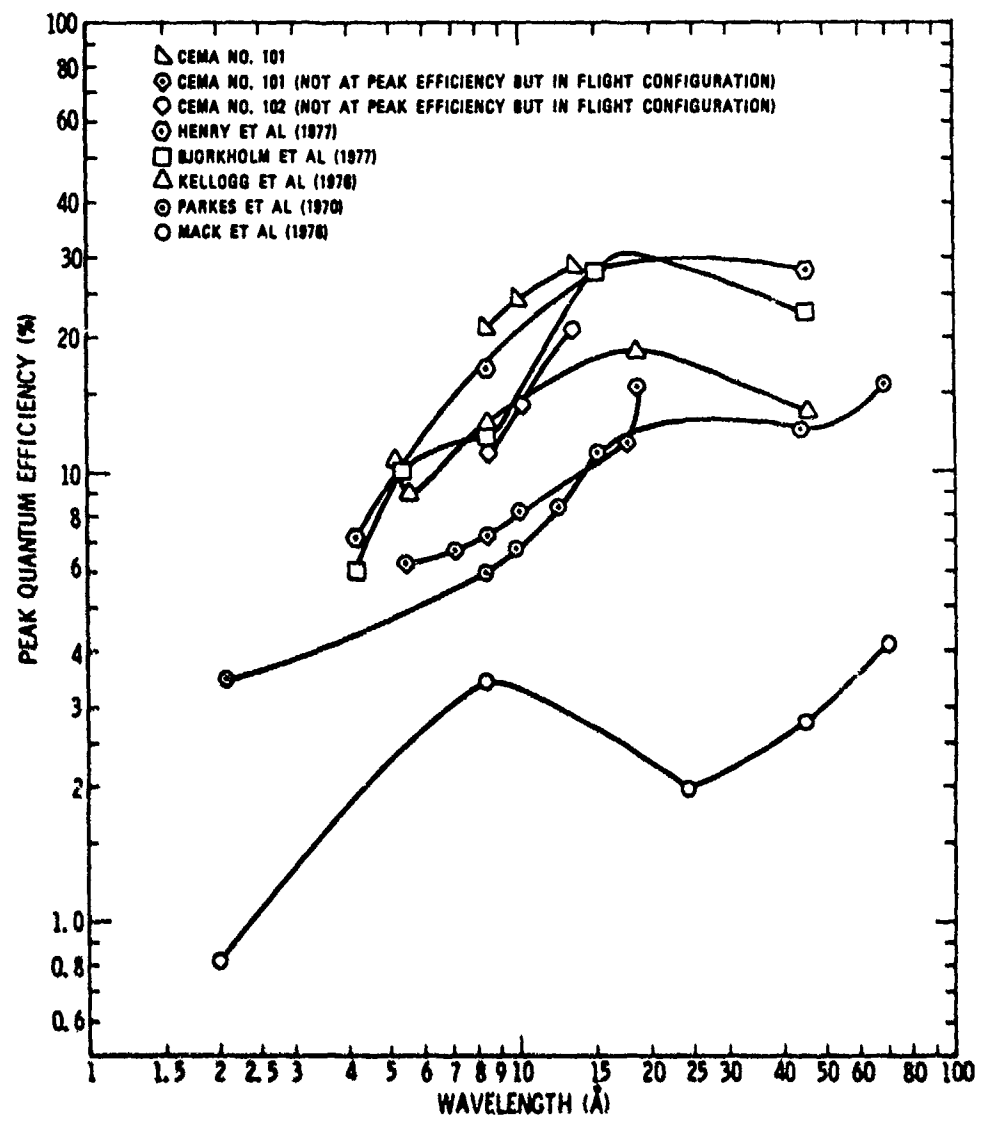
A comparison of the peak Q.E. versus wavelength curve for CEMA #101 to the same curve obtained by other experimenters is shown in Figure 17. The quantum efficiencies we obtained in the 8.34 to 13.3 \AA range peaked above those of the other investigators.

Several CEMA lifetime tests by other investigators using X-rays have been made. One study was performed by Henry et al. (1977) and their results are given in Figures 18(a) and 18(b). Henry's type V plates apparently reached a plateau or steady gain region after 10^7 counts/ mm^2 . For the type X plates, the gain decreases with increasing dose and no plateau in gain is reached. We do not know how our Galileo CEMA #101 compares in glass composition to either the Type Y or Type X plate of Henry et al. so that it is difficult to make a reasonably valid comparison. Peter Graves of Galileo (private communication) indicated that we might expect the gain to decline from about 4×10^7 to 2×10^7 during the first 10^7 total counts/ mm^2 subsequently stabilizing near the latter value until reaching about 10^{11} accumulated counts/ mm^2 (see Figures 4-7). Near this point the gain should drop rapidly. We note that in our testing of CEMA #101, we did not exceed 3.1×10^5 counts/ mm^2 (see Figures 4-7). Therefore, we have not irradiated CEMA #101 with enough X-rays to come to a definite conclusion concerning the predicted plateau effect.

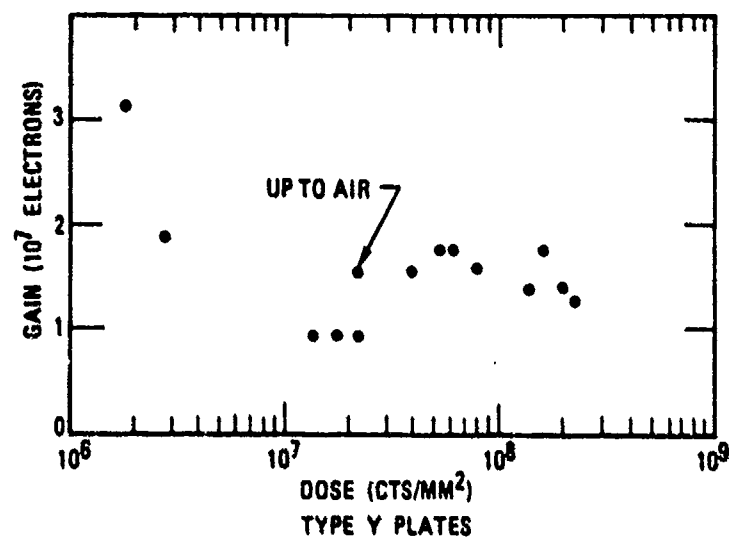
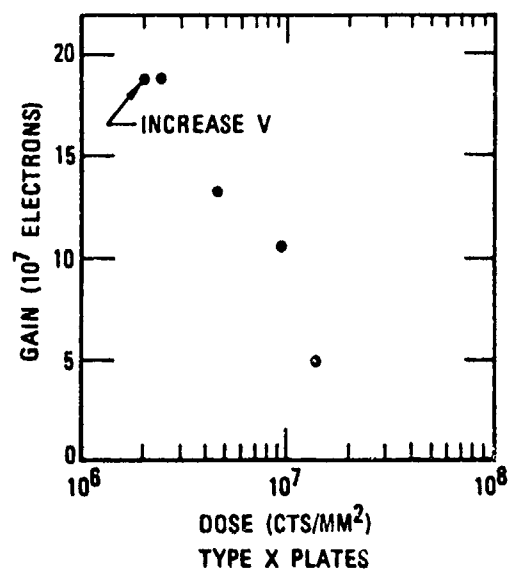
It should be recognized that studies of the long term effect of X-rays on CEMA devices have yielded different results. Sandel et al. (1977), found no period of stable gain during 2300 total hours of testing. On the other hand, Ruggieri (1972), who tested two plates for 7000 hours, found them to exhibit stable gain for the last 6000 hours. The manufacturing process of the micro-channel plates is probably responsible for such reported effects.



16. Quantum efficiency versus angular position (between CEMA normal and X-ray beam) for CEMA #101. High voltage = 2700 volts (between shield and collector). $V_{\text{front}} - V_{\text{shield}} = 30$ volts. $V_{\text{middle top}} - V_{\text{middle bottom}} = 20$ volts. Q. E. corrected for effects of shield #1. Results of Henry et al. and Bjorkholm et al. also are shown.



17. Comparison of CEMA quantum efficiency versus wavelength to that of other investigators. The effects of absorption edges have been ignored.



18. Gain versus dose for two different types of plates tested by Henry et al.

We also extensively tested CEMA #102 which, like CEMA #101, was made by Galileo. The test setup for CEMA #102 was essentially the same as shown in Figure 1 except that both the front plate and shield support were grounded and $V_{\text{middle bottom}}$ and $V_{\text{middle top}}$ were at the same voltage.

CEMA #102 can be compared with two other channel arrays for Q.E. versus angular orientation. As seen in Figure 19, the results of #102 for Al K α can be plotted along with those obtained by Henry et al. (1977) and Bjorkholm et al. (1977). The results we obtained for cathode coated CEMA #102 are nearly the same as those of Henry et al. (also coated), but higher than those of Bjorkholm et al. (uncoated). Note that if one multiplies the peak Bjorkholm et al. Q. E. on Figure 19 by 1.64, the ratio of coated to uncoated QE's given in Table II of Henry et al., all data is then in reasonably good agreement (Henry, 1981).

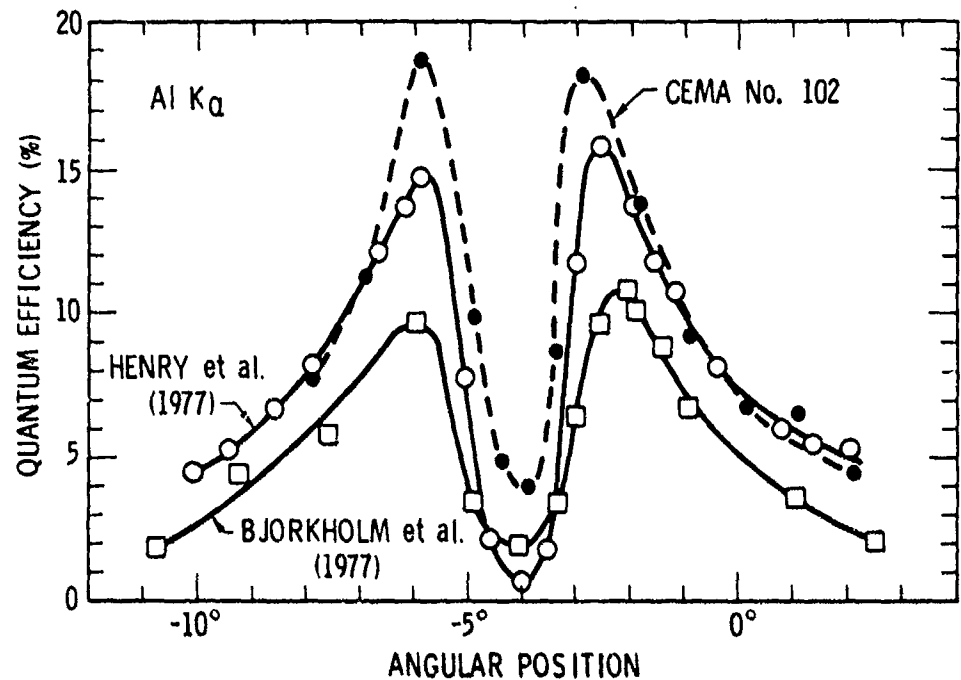
Numerous measurements were taken of CEMA #102 to establish its quantum efficiency at different wavelengths. The wavelength interval from 1.94 to 27.4 \AA was studied. The technique for measuring quantum efficiency involved using a standard P-10 gas-filled proportional counter (SPC) whose efficiency was well known over the interval.

The Q. E. formula can be expressed as:

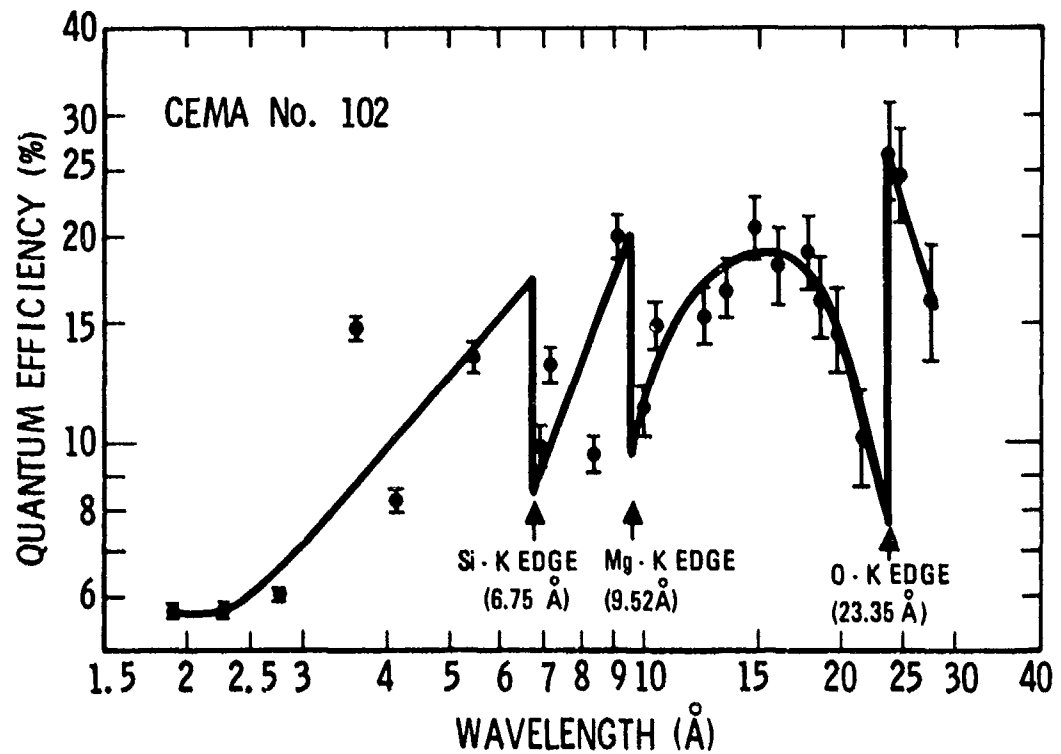
$$\text{Q. E.} = \frac{\text{CEMA collector counts} \quad \text{transmission of}}{\text{minus background counts} / \text{filters on CEMA}} \\ \frac{(\text{SPC output counts})}{(\text{efficiency of SPC})}$$

We estimated the error limits for the Q.E. by assigning the extreme possible values to the polypropylene shield covering CEMA #102 and to the aluminized mylar window on the proportional counter thereby deriving the maximum and minimum values of quantum efficiency. This was done at 23 different wavelengths between 1.94 and 27.4 \AA . The results are shown in Figure 20. There are three absorption edges of interest: 6.75 \AA (Si-K edge), 9.25 \AA (Mg-K edge), and 23.35 \AA (O-K edge).

Due to delivery constraints on flight CEMA #101, CEMA #102 was more extensively studied for Q.E. versus wavelength in the flight configuration than CEMA #101. We took the three data points for the Q.E. of CEMA #101 (AlK α , MgK α , and Cul α) and best fit them to the curve for CEMA #102, using Figure 20 as our guide. Thus, we generated a Q.E. versus wavelength curve for



19. Quantum efficiency versus angular position (between CEMA normal and X-ray beam) for CEMA #102. High voltage = 2700 volts (between shield and collector). $V_{\text{front}} = V_{\text{shield}} = V_{\text{middle top}} = V_{\text{middle bottom}} = 0$ volts. Q.E. corrected for effects of shield #8 and shield #9. Results of Henry et al. and Bjorkholm et al. are also shown. All three measurements were made with Al K α (8.34 Å).



20. Quantum efficiency versus wavelength for CEMA #102 (corrected for the effects of shield #9) in the flight configuration with appropriate error bars and absorption edges shown.

CEMA #101 in the flight configuration based on CEMA #102 data. We have presumed that the two supposedly identical CEMAs have the same response at all wavelengths.

The curve shown in Figure 21 was obtained by taking points for quantum efficiency of CEMA #101 at the same wavelengths as measured for CEMA #102, and then dividing by the appropriate transmissions for filters #10 and #12. Included in this curve are error estimates of the uncertainties involved in calculating the quantum efficiency.

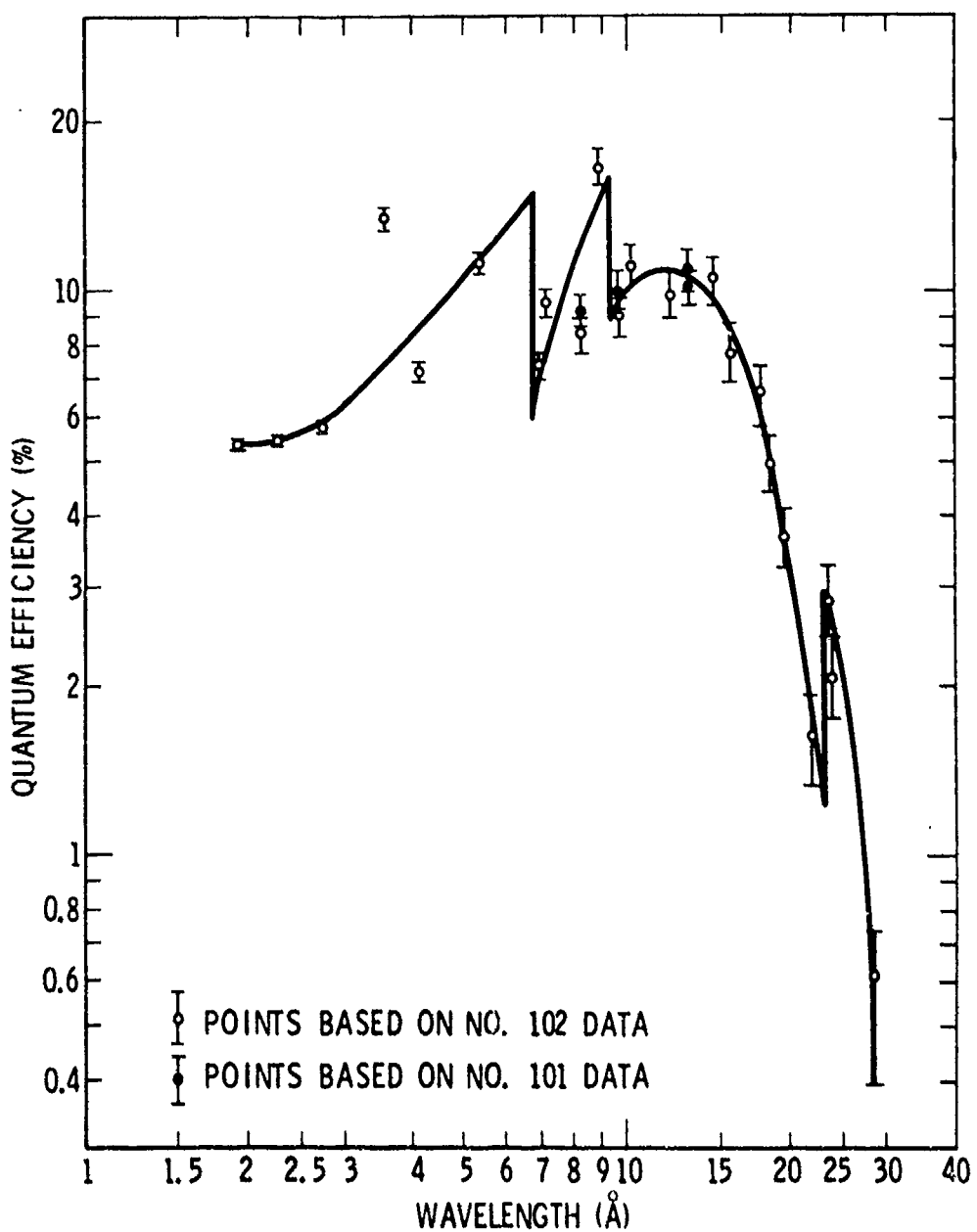
A comparison of CEMA #101 in the flight configuration with the results of other experimenters is shown in Figure 22. The curve for CEMA #101 best matches that of Kellogg et al (1976). It should be noted that we perceive three distinct x-ray K-edges from our CEMA #101. These edges are the Si K-edge (6.75 Å), the Mg K-edge (9.52 Å), and the O K-edge (23.35 Å). We find no F K-edge (18.03 Å) present in our curve although the CEMA #101 cathode was coated with MgF_2 . We recorded data at many more wavelengths than the other investigators and hence have reason to depict the three K-edges in our detailed analysis of CEMA #101. The other investigators did not have any K-edges in their Q.E. curves.

IV. SUMMARY AND CONCLUSIONS

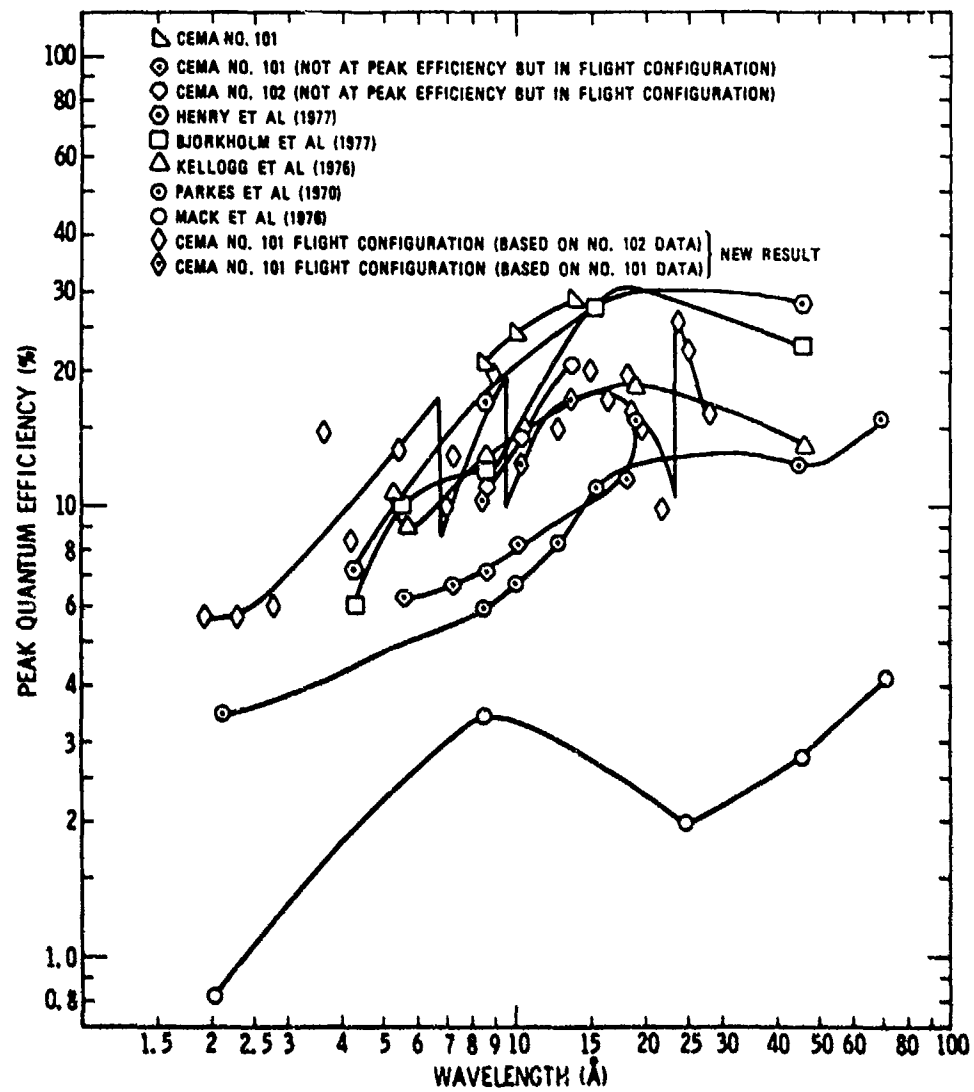
We have found the Galileo CEMA to be a useful device to measure x-rays in the 3 to 25 Å wavelength interval. The quantum efficiency of the detector, in general, is a non-linear function of wavelength with three absorption edges. The utility of CEMA #101 is dependent on the accuracy of the Q.E. versus wavelength curve, and it should be observed that at longer wavelengths the uncertainties in quantum efficiency increase due to the more marked effects of the CEMA shields on the transmission of softer x-rays.

Our detector has performed sufficiently well with regard to measurements of resolution, gain, and dark counting rate while displaying a quantum efficiency equal to or better than that of most investigators at all wavelengths measured.

Since the launch of the USAF Space Test Program P78-1 satellite on 24 February 1979, the CEMA #101 detector has operated reliably for about 10000



21. Quantum efficiency versus wavelength for CEMA #101 (taking absorption edges into account) in the flight configuration with shield #10 and #12 present.



22. Comparison of CEMA #101 quantum efficiency versus wavelength (taking absorption edges into account) with that of other investigators.

hours with no noticeable degradation. Except in the regions of high particle background, the counting rates from the onboard 9.9 \AA radioactive fluorescence calibration source have been constant ~ 120 counts/second, about the same as the pre-launch values. The high voltage power supply output ($V_{\text{collector}} - V_{\text{shield}}$) has always been in the range 2600-2620 volts since launch.

REFERENCES

Bjorkholm, P. J., L. P. Van Speybroeck, and M. Hecht, Proc. SPIE 106, 189 (1977).

Doschek, G. A., U. Feldman, P. B. Landecker, and D. L. McKenzie, Astrophys. J., (in press).

Henry, J. P., private communication (1981).

Henry, J. P., E. M. Kellogg, U. G. Briel, S. S. Murray, L. P. Van Speybroeck, and P. J. Bjorkholm, Proc. SPIE 106, 196 (1977).

Kellogg, E., P. Henry, S. Murray, and L. P. Van Speybroeck, Rev. Sci. Instr. 47, 282 (1976).

Landecker, P. B., and W. Eng, Jr., The Aerospace Corporation ATM-78(3960-01)-2, 6 pp (1978).

Landecker, P. B., W. T. Chater, C. K. Howey, D. L. McKenzie, H. R. Rugg, R. L. Williams, and R. N. Young, The Aerospace Corporation TR-0080(5960-01)-1, 210 pp. (1979a).

Landecker, P. B., D. L. McKenzie, and H. R. Rugg, Proc. SPIE 184, 285 (1979b).

Landecker, P. B., D. L. McKenzie, and H. R. Rugg, Space Research XX, 255 (1980).

Landecker, P. B. and D. L. McKenzie, Astrophys. J. Lett. 241, L175 (1980).

McKenzie, D. L., R. N. Broussard, P. B. Landecker, H. R. Rugg, R. N. Young, G. A. Doschek, and U. Feldman, Astrophys. J. Lett. 238, L43 (1980a).

McKenzie, D. L., P. B. Landecker, R. N. Broussard, H. R. Rugg, R. N. Young, U. Feldman, and G. A. Doschek, Astrophys. J. 241, 409 (1980b).

McKenzie, D. L. and P. B. Landecker, Astrophys. J., (in press).

Parkes, W., R. Gott, and K. A. Pounds, IEEE Trans. Nucl. Sci. NS-17, 360 (1970).

Ruggieri, D. J., IEEE Trans. Nucl. Sci. NS-19, 74 (1972).

Sandel, B. R., A. L. Broadfoot, and D. E. Shemansky, Applied Optics 16, 1435 (1977).

Wiza, J. L., Nucl. Instr. and Meth. 162, 587 (1979).

Wiza, J. L., P. R. Henkel, and R. L. Roy, Rev. Sci. Instr. 48, 1217 (1977).

LABORATORY OPERATIONS

The Laboratory Operations of The Aerospace Corporation is conducting experimental and theoretical investigations necessary for the evaluation and application of scientific advances to new military concepts and systems. Versatility and flexibility have been developed to a high degree by the laboratory personnel in dealing with the many problems encountered in the Nation's rapidly developing space systems. Expertise in the latest scientific developments is vital to the accomplishment of tasks related to these problems. The laboratories that contribute to this research are:

Aerophysics Laboratory: Aerodynamics; fluid dynamics; plasmadynamics; chemical kinetics; engineering mechanics; flight dynamics; heat transfer; high-power gas lasers, continuous and pulsed, IR, visible, UV; laser physics; laser resonator optics; laser effects and countermeasures.

Chemistry and Physics Laboratory: Atmospheric reactions and optical backgrounds; radiative transfer and atmospheric transmission; thermal and state-specific reaction rates in rocket plumes; chemical thermodynamics and propulsion chemistry; laser isotope separation; chemistry and physics of particles; space environmental and contamination effects on spacecraft materials; lubrication; surface chemistry of insulators and conductors; cathode materials; sensor materials and sensor optics; applied laser spectroscopy; atomic frequency standards; pollution and toxic materials monitoring.

Electronics Research Laboratory: Electromagnetic theory and propagation phenomena; microwave and semiconductor devices and integrated circuits; quantum electronics, lasers, and electro-optics; communication sciences, applied electronics, superconducting and electronic device physics; millimeter-wave and far-infrared technology.

Materials Sciences Laboratory: Development of new materials; composite materials; graphite and ceramics; polymeric materials; weapons effects and hardened materials; materials for electronic devices; dimensionally stable materials; chemical and structural analyses; stress corrosion; fatigue of metals.

Space Sciences Laboratory: Atmospheric and ionospheric physics, radiation from the atmosphere, density and composition of the atmosphere, aurorae and airglow; magnetospheric physics, cosmic rays, generation and propagation of plasma waves in the magnetosphere; solar physics, x-ray astronomy; the effects of nuclear explosions, magnetic storms, and solar activity on the earth's atmosphere, ionosphere, and magnetosphere; the effects of optical, electromagnetic, and particulate radiations in space on space systems.

• • •